

# Resolution enhancement of imaging small-scaled portions in a compactly-support function

Hsin M. Shieh,<sup>1,\*</sup> Yu-Ching Hsu,<sup>1</sup> Charles L. Byrne,<sup>2</sup>

and Michael A. Fiddy<sup>3</sup>

<sup>1</sup>*Department of Electrical Engineering, Feng Chia University,  
100 Wenhwa Rd., Seatwen, Taichung, Taiwan 40724, R.O.C.*

<sup>2</sup>*Department of Mathematical Sciences, University of Massachusetts Lowell,  
One University Avenue, Lowell, MA 01854, U.S.A.*

<sup>3</sup>*Center for Optoelectronics and Optical Communications,  
The University of North Carolina at Charlotte,  
9201 University City Blvd., Charlotte, NC 28223, U.S.A.*

*\*Corresponding author: hmshieh@fcu.edu.tw*

The ambiguity involved in reconstructing an image from limited Fourier data is removed using a new technique that incorporates prior knowledge of the location of regions containing small-scale features of interest. The “prior discrete Fourier transform” (PDFT) method for image reconstruction incorporates prior knowledge of the support, and perhaps general shape, of the object function being reconstructed through the use of a weight function. The new approach extends the PDFT by allowing different weight functions to modulate the different spatial frequency components of the reconstructed image. The effectiveness of the new method is tested on one- and two-dimensional simulations. © 2009 Optical Society of America

*OCIS codes:* 100.3010, 100.3020, 100.3190, 100.6640.

## 1. Introduction

Many image reconstruction techniques have been remarkably successful in applications such as medical imaging, remote sensing, nondestructive testing, and radar. Here our focus is on a general problem that arises in many such applications, the reconstruction of a compactly-supported function from a limited number of its Fourier-transform values. Because the data is limited, there are an infinite number of solutions consistent with the data [1, 2], and it is typically challenging to choose a good image estimate. Among all data-consistent estimates, the well-known minimum-norm (MN) estimation takes the one which has the smallest energy. A special case of the MN estimation,

referred to as the discrete Fourier transform (DFT), can be easily and efficiently implemented with a finite-length data vector of uniformly-sampled Fourier transform values by the fast Fourier transform (FFT), but usually fails to achieve an acceptable resolution for fine-structured object. As is properly understood, the degree of freedom from finitely sampled Fourier data limits the DFT resolution [2, 3]. High-resolution methods, such as Gerchberg-Papoulis band-limited extrapolation [4, 5] and Burg's maximum-entropy spectral-estimation [6–8], can present a superiority of resolving the details of fine-structured object to the DFT, through the incorporation of some known aspect (piori) about the object to be reconstructed. Of particular interest in this paper is the model based on the minimum weighted norm (MWN) estimation. In particular, to combat a more challenging problem of imaging small-scaled portions in a compactly-support function, we present a promising image reconstruction method.

It is often the goal to image accurately some small and finer portion of the object. This critical issue is much harder, especially when the small-scale portions involve only a small amount of the total energy from the object. Our topic here is the reconstruction of such small-scale features of a compactly-supported function, from values of its Fourier transform. We develop a new imaging technique in which the reconstructed image is a weighted sum of windowed complex exponential functions. The resolution enhancement comes from the incorporation of prior knowledge of the domain of the object, as well as the locations of the small-scale features of interest. The coefficients in the sum are determined by imposing the condition that the reconstructed image

be consistent with the measured data. We use uniform-amplitude windows, although smooth-shaped windows may lead to smoother reconstructions. Our proposed algorithm is closely related to the prior discrete Fourier transform (PDFFT) reconstruction method [9–16]. The effectiveness of our method is illustrated in several examples.

## 2. Mathematical Background

Let  $f(x)$  be a complex-valued function supported on the interval  $[-\pi, \pi]$  of the real line. Let the data be the Fourier-transform values

$$F(k_n) = \int_{-\pi}^{\pi} f(x) \exp(-jxk_n) dx , \quad (1)$$

for  $n = 1, 2, \dots, N$ . Our reconstruction will take the form of a linear estimator of  $f(x)$ ,

$$\hat{f}(x) = \sum_{n=1}^N a_n b_n(x) , \quad (2)$$

where the  $b_n(x)$  are known functions and the  $a_n$  are determined by the data-consistency conditions. For example, if  $k_n = 2\pi n/N$ , and  $b_n(x) = \exp(jxk_n)$ , then Eqn. (2) becomes

$$\hat{f}(x) = \frac{1}{2\pi} \sum_{n=1}^N F(k_n) \exp(jxk_n) , \quad (3)$$

which is the minimum-norm reconstruction, also called the DFT reconstruction. The DFT method is easily implemented using the Fast Fourier Transform (FFT).

Suppose that the true object function  $f(x)$  takes the value zero for  $|x| > \nu$ , for some  $\nu$  in the interval  $(0, \pi)$ . Except when  $N$  is large, the DFT usually provides a poor reconstruction, since it does not incorporate the knowledge that the support of  $f(x)$  is limited to the interval  $[-\nu, \nu]$ .

To incorporate prior knowledge of the support of  $f(x)$ , we select a non-negative function  $w(x)$  supported on a set  $\Omega$  containing the interval  $[-\nu, \nu]$ , and find the function of the form

$$\hat{f}_{\text{PDFT}}(x) = w(x) \sum_{n=1}^N a_n \exp(jxk_n); \quad (4)$$

this is the “prior discrete Fourier transform” (PDFT) reconstruction.

To satisfy the data-consistency requirements, we must have

$$F(k_m) = \sum_{n=1}^N a_n W(k_m - k_n), \quad (5)$$

for  $m = 1, 2, \dots, N$ , where  $W(k)$  is the Fourier transform of the function  $w(x)$ . A typical choice for  $w(x)$  is the function  $w(x) = \chi_{\Omega}(x)$  that takes the value one for  $x$  in  $\Omega$ , and zero outside  $\Omega$ . The closer the set  $\Omega$  is to the interval  $[-\nu, \nu]$ , the better the reconstruction, although care must be taken to regularize in the case of noisy data.

With  $w(x) = \chi_{\Omega}(x)$ , let  $P_{\Omega}$  be the matrix with entries  $P_{m,n} = W(k_m - k_n)$ . Then  $P_{\Omega}$  is a positive-definite Hermitian matrix with positive eigenvalues  $\lambda_1 > \lambda_2 > \dots > \lambda_N$  and associated norm-one eigenvectors  $u_1, u_2, \dots, u_N$ . The PDFT reconstruction of

$f(x)$  in Eqn. (4) can then be written

$$\hat{f}_{\text{PDFT}}(x) = \chi_{\Omega}(x) \sum_{n=1}^N \lambda_n^{-1} (u_n^\dagger F) U_n(x), \quad (6)$$

where  $F$  is the column vector with entries  $F(k_n)$ ,

$$U_n(x) = \sum_{m=1}^M (u_n)_m \exp(jxk_m), \quad (7)$$

and  $(u_n)_m$  is the  $m$ -th entry of the vector  $u_n$ . Because the eigenvectors of  $P_{\Omega}$  are orthogonal, it follows that

$$\int_{\Omega} U_n(x) \overline{U_m(x)} dx = \lambda_n u_m^\dagger u_n = 0 \quad (8)$$

for  $m \neq n$ , and

$$\int_{\Omega} |U_n(x)|^2 dx = \lambda_n. \quad (9)$$

From these equations we learn that the  $U_n(x)$ , which we call here the “eigenfunctions”, are mutually orthogonal functions within the set  $\Omega$ , and as  $n$  increases, the functions  $U_n(x)$  become less concentrated within  $\Omega$  and possess more zeros at values of  $x$  within  $\Omega$ . This means that, for the higher values of  $n$ , the functions  $U_n(x)$  oscillate more rapidly within  $\Omega$ . Because the PDFT reconstruction also employs the weights  $\lambda_n^{-1}$ , the functions  $U_n(x)$  with the most oscillation within  $\Omega$  are the ones that are

most prominent in the reconstruction, thereby increasing the resolution (see Shieh et al.). When the amount of data is large, forming the matrix  $P_\Omega$  can be prohibitively expensive. In such cases, the use of the matrix  $P_\Omega$  can be avoided and the PDFFT reconstruction can be calculated using an iterative weighted algebraic reconstruction technique (see Shieh et al.).

Even with accurate prior information about the true object support, the PDFFT may not reconstruct small-scale features with the necessary accuracy. To achieve improved resolution of such small-scale features, we modify the PDFFT reconstruction and select an estimate of  $f(x)$  having the form

$$\hat{f}(x) = \sum_{n=1}^N a_n w_n(x) \exp(jxk_n), \quad (10)$$

where the  $w_n(x)$  are selected non-negative window functions. Data consistency is achieved when the  $a_n$  satisfy the equations

$$F(k_m) = \sum_{n=1}^N a_n W_n(k_m - k_n), \quad (11)$$

where  $W_n(k)$  is the Fourier transform of  $w_n(x)$ .

### 3. Selection of windows

Suppose that the support of  $f(x)$ , which we take to equal  $\Omega$ , can be divided into two disjoint regions, a larger one, denoted  $L$ , in which there are no small-scale features,

and a smaller one, denoted  $S$ , containing small-scale features of interest to us. Suppose also that the set  $\{k_n\}$  of “spatial frequencies” can be divided into two sets,  $LF$  and  $HF$ , with  $LF = \{k_n | n = 1, \dots, K\}$  consisting of lower values of  $k_n$  and  $HF = \{k_n | n = K + 1, \dots, N\}$  consisting of higher values.

Our PDFT reconstructed image is

$$\hat{f}_{\text{PDFT}}(x) = \chi_L(x) \sum_{n=1}^N a_n \exp(jxk_n) + \chi_S(x) \sum_{n=1}^N a_n \exp(jxk_n), \quad (12)$$

using

$$\chi_\Omega(x) = \chi_L(x) + \chi_S(x).$$

If we can safely assume that within the set  $L$  the function  $f(x)$  involves no high spatial frequencies, and within the set  $S$  no low spatial frequencies, then it makes sense to modify Eqn. (12) and write

$$\hat{f}(x) = \chi_L(x) \sum_{n|k_n \in LF} a_n \exp(jxk_n) + \chi_S(x) \sum_{n|k_n \in HF} a_n \exp(jxk_n). \quad (13)$$

Suppose, just for the sake of getting some feeling for what is going on here, we make the simplifying assumption that

$$\int_L \exp(jxk_n) \exp(-jxk_m) dx = \int_S \exp(jxk_m) \exp(-jxk_n) dx = 0, \quad (14)$$

whenever  $k_n \in LF$  and  $k_m \in HF$ . Then the matrix involved in the system of equations to be solved is block-diagonal, with  $P_L$  in the northwest block and  $P_S$  in the southeast block. As a result, the reconstruction given by Eqn. (13) will be a sum of the  $U_n(x)$  for the matrix  $P_L$ , for  $x$  in  $L$ , and the  $U_n(x)$  for the matrix  $P_S$ , for  $x$  in  $S$ . Since  $\chi_S(x)$  has the small set  $S$  for its support, the eigenfunctions  $U_n(x)$  associated with  $P_S$  oscillate rapidly within the set  $S$ , allowing the reconstruction to reveal small-scale detail within that region.

The reconstruction in Eqn. (10) simply extends this idea, allowing each spatial frequency to have its own region, although, in practice, there will usually be only two distinct windows, as in our illustration. For the purpose of explanation, one- and two-dimensional examples are demonstrated in the following two sections.

#### 4. Some one-dimensional simulations

For the one-dimensional simulations, let's assume that 31 low-pass Fourier transform values of frequencies,  $\{-15, \dots, 0, \dots, 15\}$ , are used in the image reconstruction. A typical case is that the object is characterized as a small and finer part embedded in a large smooth background, as shown in Fig. 1 and Fig. 2. To obtain a good image by our proposed method, window functions  $w_n$  can be chosen as either  $\chi_S$  for confining complex exponentials of frequencies  $\{k_n \mid |k_n| \geq |k_{th}|, \text{ for } n = 1, 2, \dots, 31\}$ , or  $\chi_L$  for complex exponentials of other frequencies  $\{k_n \mid |k_n| < |k_{th}|, \text{ for } n = 1, 2, \dots, 31\}$ . In principle,  $\chi_\Omega (\chi_S + \chi_L)$  must agree with the object's true domain accurately, and this

true domain can be typically acquired for some applications, such as medical imaging and nuclear power plant nondestructive flaw testing. As shown in Fig. 2(c), if assigning  $\chi_L$  (2(a)) for complex exponentials of frequencies  $\{-11, \dots, 0, \dots, 11\}$  ( $k_{th} = 11$ ) and  $\chi_S$  (2(b)) for otherwise, our proposed technique can obtain a good-quality image, clearly superior to the DFT estimate in Fig. 1(a) and the PDFFT estimate in Fig. 1(c) with a tight prior ( $\chi_\Omega$ ) in Fig. 1(b).

In our proposed method, the support domain of  $\chi_S$  is critical to the final image estimate. In essence,  $\chi_S$  having a more accurate support to the small portion's domain can typically lead to a higher-quality image reconstruction, but  $\chi_S$  must cover the small portion's domain for an acceptable image at least. With the same object and sampled Fourier data used in Fig. 1 and Fig. 2, the examples of poorly-using and misusing  $\chi_S$  are shown in Fig. 3, Fig. 4, Fig. 5, and Fig. 6.

For more realistic situation in applications, there can be typically several discrete small portions within the object. In Fig. 7 and Fig. 8, for the purpose of demonstration, two discrete finer portions with different profiles are inset in the object. The choice of  $\chi_S$  can be suitably discretely-distributed windows wherein each window accommodates a finer part individually. For the estimate in Fig. 8(c), with  $\chi_L$  in Fig. 8(a),  $\chi_S$  in Fig. 8(b), and  $k_{th} = 9$ , our proposed method essentially presents its superiority over the DFT estimate in Fig. 7(a) and the PDFFT estimate in Fig. 7(c). While a simple example having only two discrete small portions is demonstrated here, this strategic choice of window functions can be easily extended for the case with more

discrete finer portions.

The determination of an appropriate value of  $k_{th}$  is somewhat challenging for our proposed method. In principle, taking an improper value of  $k_{th}$  forces some/all windowed exponentials to reconstruct the image over unappropriate regions, and consequently boost up the energy of the resulting estimate mistakenly. Accordingly, for quantitative purpose, the Frobenius norm (Hilbert-Schmidt norm) of the final estimate by our proposed method can be used as a measure of appropriateness. For the example in Fig. 2, the chart of the image estimate's norm with respect to  $k_{th}$  is shown in Fig. 9, in which the values of  $k_{th}$  between 8 and 13 physically correspond to a more or less minimum norm and obtain good-quality images (10 is the best for this example). Additionally, for the example in Fig. 8, the chart of the image estimate's norm with respect to  $k_{th}$  is shown in Fig. 10, and the values between 6 and 11 are acceptable (7 is the best).

## 5. Some two-dimensional simulations

The extension of our proposed technique to the two-dimensional problem is straightforward. Let the two-dimensional object function  $f(x, y)$  be compactly supported in  $|x| \leq \pi$  and  $|y| \leq \pi$ , and have its sampled Fourier transform values given by

$$F(\alpha_m, \beta_n) = \int_{-\pi}^{\pi} \int_{-\pi}^{\pi} f(x, y) \exp(-jx\alpha_m - jy\beta_n) dx dy, \quad (15)$$

for  $m = 1, 2, \dots, M$  and  $n = 1, 2, \dots, N$ . The two-dimensional algorithm is formulated as

$$\hat{f}(x, y) = \sum_{m=1}^M \sum_{n=1}^N a_{m,n} w_{m,n}(x, y) \exp(jx\alpha_m + jy\beta_n), \quad (16)$$

and the weights  $a_{m,n}$  for  $n = 1, 2, \dots, N$  can be determined by

$$F(\alpha_p, \beta_q) = \sum_{m=1}^M \sum_{n=1}^N a_{m,n} W_{m,n}(\alpha_p - \alpha_m, \beta_q - \beta_n), \quad (17)$$

for  $p = 1, 2, \dots, M$  and  $q = 1, 2, \dots, N$ .  $W_{m,n}$  is the Fourier transform of  $w_{m,n}$ .

To test the above two-dimensional modality, we applied it to Fourier transform data of frequencies located in a  $31 \times 31$  square regular grid. The window functions  $w_{m,n}(x, y)$ , for  $m = 1, 2, \dots, M$  and  $n = 1, 2, \dots, N$ , are chosen in the following manner,

$$w_{m,n}(x, y) = \begin{cases} \chi_L, & \text{for } \sqrt{\alpha_m^2 + \beta_n^2} \leq k_{th} \\ \chi_S, & \text{otherwise} \end{cases}$$

where the two-dimensional uniform-amplitude window  $\chi_D$  takes the value one for  $(x, y)$  in  $D$ , and zero outside  $D$ .

For the two-dimensional simulations, the object to be reconstructed is shown in Fig. 11(a), and the DFT estimate in Fig. 11(b) gives a poor resolution. With a tight prior window in Fig. 11(c), the PDFFT estimate in Fig. 11(d) does not improve the image quality much, especially for small circular spots. If taking a window function  $\chi_L$  in Fig. 12(a) for complex exponentials of frequencies  $\{(\alpha_m, \beta_n) \mid \sqrt{\alpha_m^2 + \beta_n^2} \leq$

13, for  $m = 1, 2, \dots, M$  and  $n = 1, 2, \dots, N$ } and a window  $\chi_s$  in Fig. 12(b) for otherwise, the estimate by our proposed method in Fig. 12(c) improves a better resolution indeed, as compare to the DFT and PDFT estimates.

## 6. Conclusions

We have presented a new approach to resolving small-scale features within a portion of a compactly-supported function from limited Fourier-transform values. In the simplest case, we divide the exponential basis functions into two groups, according to the values of their spatial frequencies, and multiply those in each group by the window function corresponding either to the region of containing no small-scale features, or the region containing such features. Comparisons are made with the DFT and PDFT reconstructions, using simulated data and the Frobenius norm measure. While the new method shows promise, it remains to test it on noisy data and to develop suitable regularization methods.

## References

1. M. Bertero and P. Boccacci, *Introduction to inverse problems in imaging* (IOP Publishing, Bristol and Philadelphia, 1998).
2. C. L. Byrne, *Signal Processing: A Mathematical Approach* (AK Peters, Ltd., Wellesley, MA, 2005).
3. M. Bertero, "Sampling theory, resolution limits and inversion methods," in "In-

- verse problems in scattering and imaging,” , M. Bertero and E. R. Pike, eds. (Malvern Physics Series, Adam Hilger, IOP Publishing, 1992), pp. 71–94.
4. R. W. Gerchberg, “Super-restoration through error energy reduction,” *Opt. Acta* **21**, 709–720 (1974).
  5. A. Papoulis, “A new algorithm in spectral analysis and band-limited extrapolation,” *IEEE Trans. Circuits Syst.* **22**, 735–742 (1975).
  6. J. P. Burg, “Maximum entropy spectral analysis,” in “the 37th Annual Society of Exploration Geophysicists Meeting,” (Oklahoma City, Oklahoma, 1967).
  7. J. P. Burg, “The relationship between maximum entropy spectra and maximum likelihood spectra,” *Geophysics* **37**, 375–376 (1972).
  8. J. P. Burg, “Maximum entropy spectral analysis,” Ph.D. thesis, Stanford University, Stanford, California (1975).
  9. C. L. Byrne and R. M. Fitzgerald, “Reconstruction from partial information, with applications to tomography,” *SIAM J. Appl. Math.* **42**, 933–940 (1982).
  10. C. L. Byrne, R. M. Fitzgerald, M. A. Fiddy, T. J. Hall, and A. M. Darling, “Image restoration and resolution enhancement,” *J. Opt. Soc. Am.* **73**, 1481–1487 (1983).
  11. C. L. Byrne and R. M. Fitzgerald, “Spectral estimators that extend the maximum entropy and maximum likelihood methods,” *SIAM J. Appl. Math.* **44**, 425–442 (1984).
  12. C. L. Byrne and M. A. Fiddy, “Estimation of continuous object distributions

from limited Fourier magnitude measurements,” *J. Opt. Soc. Am. A* **4**, 112–117 (1987).

13. C. L. Byrne and M. A. Fiddy, “Image as power spectral; reconstruction as a Wiener filter approximation,” *Inverse Problems* **4**, 399–409 (1988).
14. T. J. Hall, A. M. Darling, and M. A. Fiddy, “Image compression and restoration incorporating prior knowledge,” *Optics Letters* **7**, 467–468 (1982).
15. H. M. Shieh, C. L. Byrne, and M. A. Fiddy, “Image reconstruction: a unifying model for resolution enhancement and data extrapolation. Tutorial,” *J. Opt. Soc. Am. A* **23**, 258–266 (2006).
16. H. M. Shieh and M. A. Fiddy, “Accuracy of extrapolated data as a function of prior knowledge and regularization,” *Appl. Opt.* **45**, 3283–3288 (2006).

## List of Figure Captions

Fig. 1. An example of reconstructing a one-dimensional object function (solid line) by the DFT and PDFT, (a) the DFT estimate (dotted line), (b) the prior function (dashed line), and (c) the PDFT estimate (dotted line) with the prior in (b).

Fig. 2. An example of reconstructing a one-dimensional object function (solid line) by our proposed method, (a) the window function  $\chi_L$  (dashed line), (b) the window function  $\chi_S$  (dashed line), and (c) the estimate by our proposed method (dotted line) with  $\chi_L$  in (a) for complex exponentials of frequencies  $\{-10, \dots, 0, \dots, 10\}$  and  $\chi_S$  in (b) for otherwise.

Fig. 3. An example of reconstructing a one-dimensional object function (solid line) using a properly-located but poorly-sized window (too wide) as  $\chi_S$  in our proposed method, (a) the window function  $\chi_L$  (dashed line), (b) the window function  $\chi_S$  (dashed line), and (c) the best estimate (dotted line) with window functions  $\chi_L$  in (a) and  $\chi_S$  in (b).

Fig. 4. An example of reconstructing a one-dimensional object function (solid line) using a properly-located but improperly-sized window (too narrow) as  $\chi_S$  in our proposed method, (a) the window function  $\chi_L$  (dashed line), (b) the window function  $\chi_S$  (dashed line), and (c) the best estimate (dotted line) with window functions  $\chi_L$  in (a) and  $\chi_S$  in (b).

Fig. 5. An example of reconstructing a one-dimensional object function (solid line)

using a properly-sized but improperly-located window as  $\chi_S$  ( $\chi_S$  cannot cover the small portion of interest completely) in our proposed method, (a) the window function  $\chi_L$  (dashed line), (b) the window function  $\chi_S$  (dashed line), and (c) the best estimate (dotted line) with window functions  $\chi_L$  in (a) and  $\chi_S$  in (b).

Fig. 6. An example of reconstructing a one-dimensional object function (solid line) using a properly-sized but improperly-located window as  $\chi_S$  ( $\chi_S$  does not cover the small portion of interest at all) in our proposed method, (a) the window function  $\chi_L$  (dashed line), (b) the window function  $\chi_S$  (dashed line), and (c) the best estimate (dotted line) with window functions  $\chi_L$  in (a) and  $\chi_S$  in (b).

Fig. 7. An example of reconstructing a one-dimensional object function (solid line) by the DFT and PDFDT, (a) the DFT estimate (dotted line), (b) the prior function (dashed line), and (c) the PDFDT estimate (dotted line) with the prior in (b).

Fig. 8. An example of reconstructing a one-dimensional object function (solid line) by our proposed method, (a) the window function  $\chi_L$  (dashed line), (b) the window function  $\chi_S$  (dashed line), and (c) the estimate by our proposed method (dotted line) with  $\chi_L$  in (a) for complex exponentials of frequencies  $\{-7, \dots, 0, \dots, 7\}$  and  $\chi_S$  in (b) for otherwise.

Fig. 9. The norms of the image estimate by our proposed method with respect to  $k_{th}$  for the example in Fig. 2.

Fig. 10. The norms of the image estimate by our proposed method with respect to  $k_{th}$  for the example in Fig. 8.

Fig. 11. An example of reconstructing a two-dimensional object function by the DFT and PDFFT, (a) the object, (b) the DFT estimate, (c) the prior function, and (d) the PDFFT estimate with the prior in (c).

Fig. 12. An example of reconstructing a two-dimensional object function by our proposed method, (a) the window function  $\chi_L$ , (b) the window function  $\chi_S$ , and (c) the estimate by our proposed method with  $\chi_L$  in (a) for complex exponentials of frequencies  $\{(\alpha_m, \beta_n) \mid \sqrt{\alpha_m^2 + \beta_n^2} \leq 13, \text{ for } m = 1, 2, \dots, M \text{ and } n = 1, 2, \dots, N\}$  and  $\chi_S$  in (b) for otherwise.

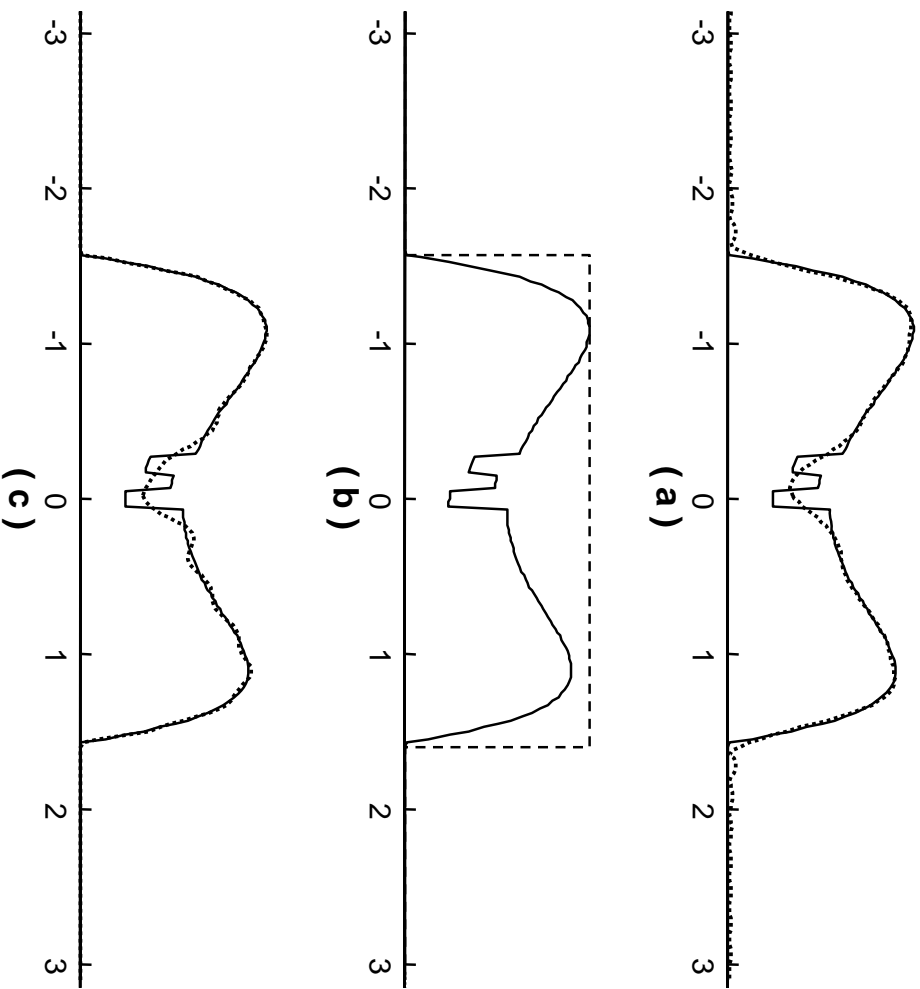


Fig. 1. An example of reconstructing a one-dimensional object function (solid line) by the DFT and PDFT, (a) the DFT estimate (dotted line), (b) the prior function (dashed line), and (c) the PDFT estimate (dotted line) with the prior in (b). Shieh\_01.eps

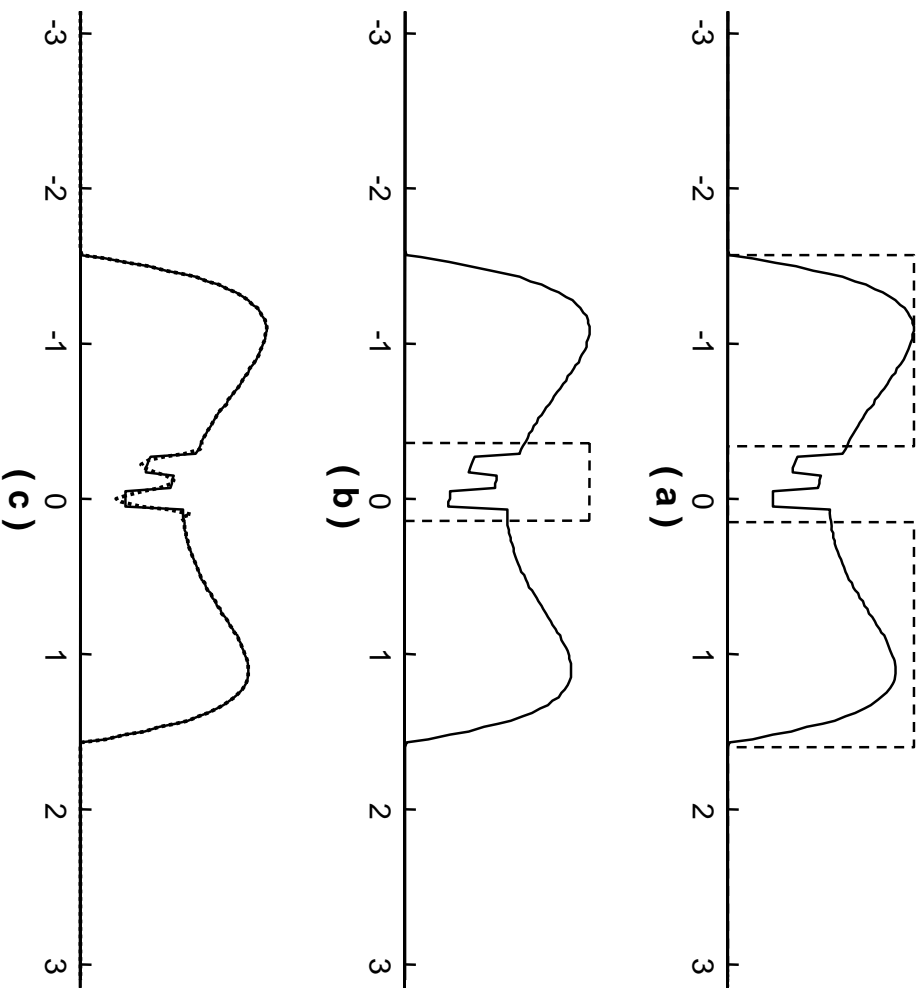


Fig. 2. An example of reconstructing a one-dimensional object function (solid line) by our proposed method, (a) the window function  $X_L$  (dashed line), (b) the window function  $X_S$  (dashed line), and (c) the estimate by our proposed method (dotted line) with  $X_L$  in (a) for complex exponentials of frequencies  $\{-10, \dots, 0, \dots, 10\}$  and  $X_S$  in (b) for otherwise. Shieh\_02.eps

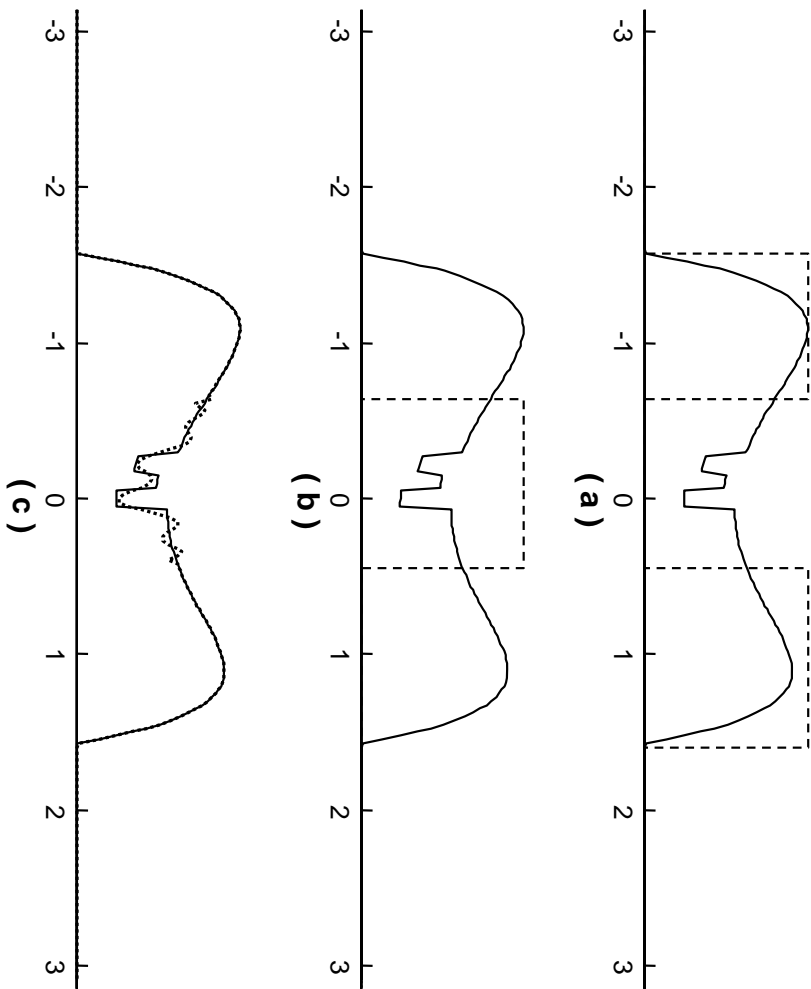


Fig. 3. An example of reconstructing a one-dimensional object function (solid line) using a properly-located but poorly-sized window (too wide) as  $\chi_S$  in our proposed method, (a) the window function  $\chi_L$  (dashed line), (b) the window function  $\chi_S$  (dashed line), and (c) the best estimate (dotted line) with window functions  $\chi_L$  in (a) and  $\chi_S$  in (b). Shieh\_03.eps

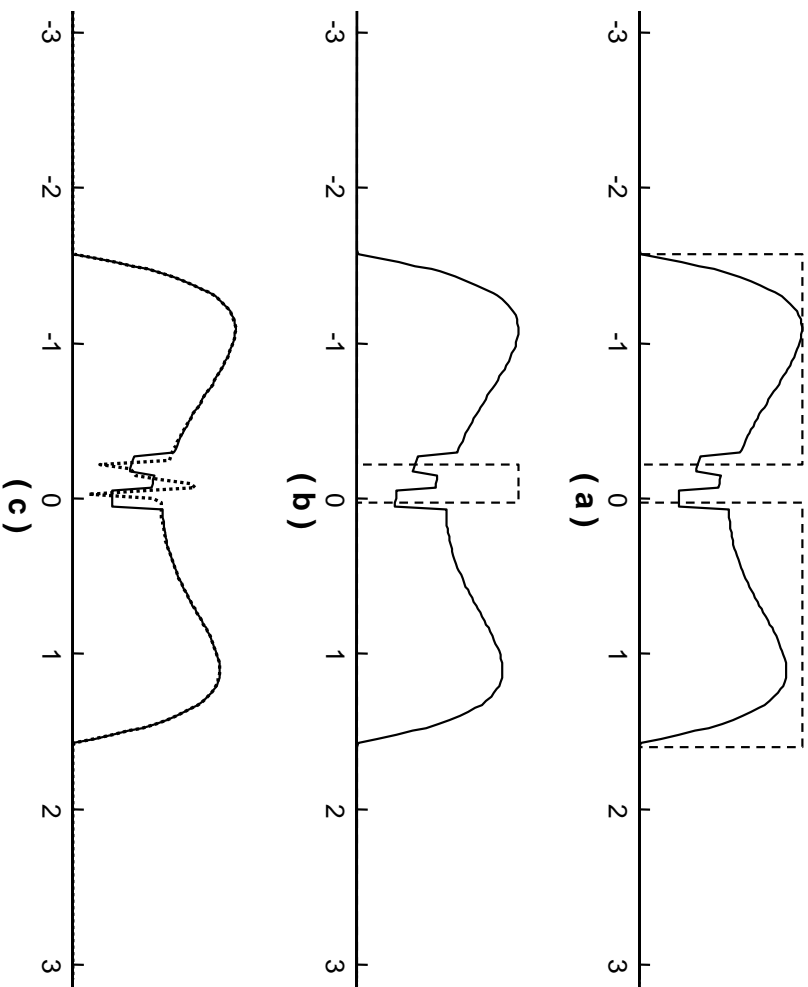


Fig. 4. An example of reconstructing a one-dimensional object function (solid line) using a properly-located but improperly-sized window (too narrow) as  $\chi_S$  in our proposed method, (a) the window function  $\chi_L$  (dashed line), (b) the window function  $\chi_S$  (dashed line), and (c) the best estimate (dotted line) with window functions  $\chi_L$  in (a) and  $\chi_S$  in (b). Shieh\_04.eps

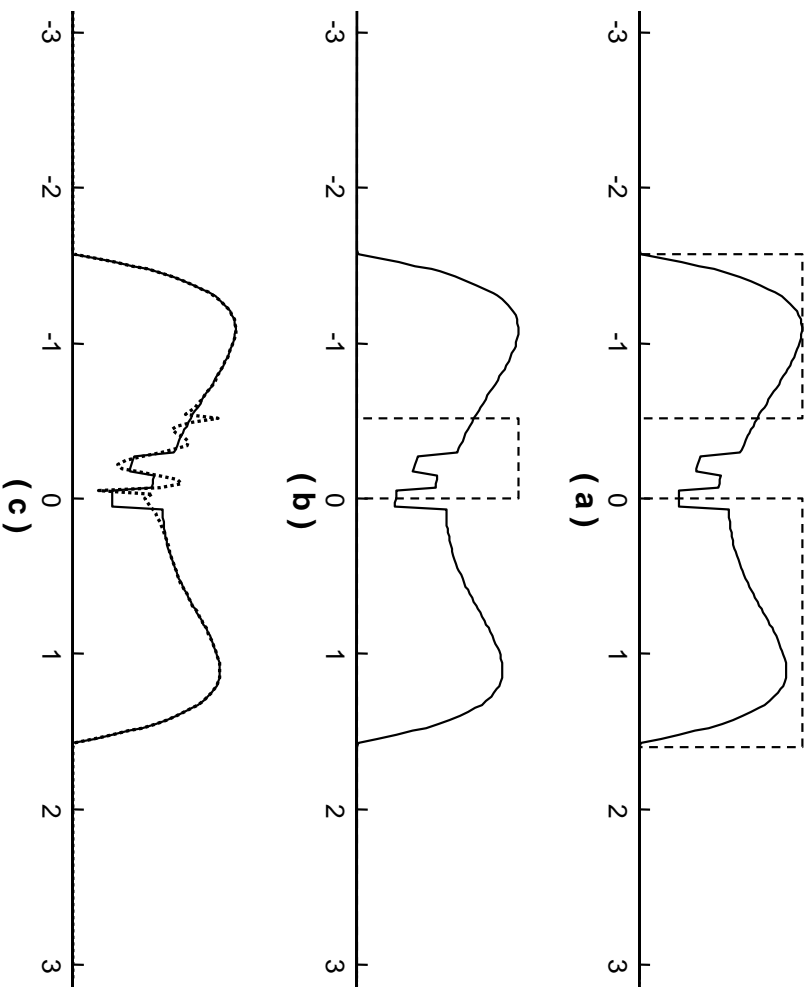


Fig. 5. An example of reconstructing a one-dimensional object function (solid line) using a properly-sized but improperly-located window as  $\chi_S$  ( $\chi_S$  cannot cover the small portion of interest completely) in our proposed method, (a) the window function  $\chi_L$  (dashed line), (b) the window function  $\chi_S$  (dashed line), and (c) the best estimate (dotted line) with window functions  $\chi_L$  in (a) and  $\chi_S$  in (b). Shieh\_05.eps

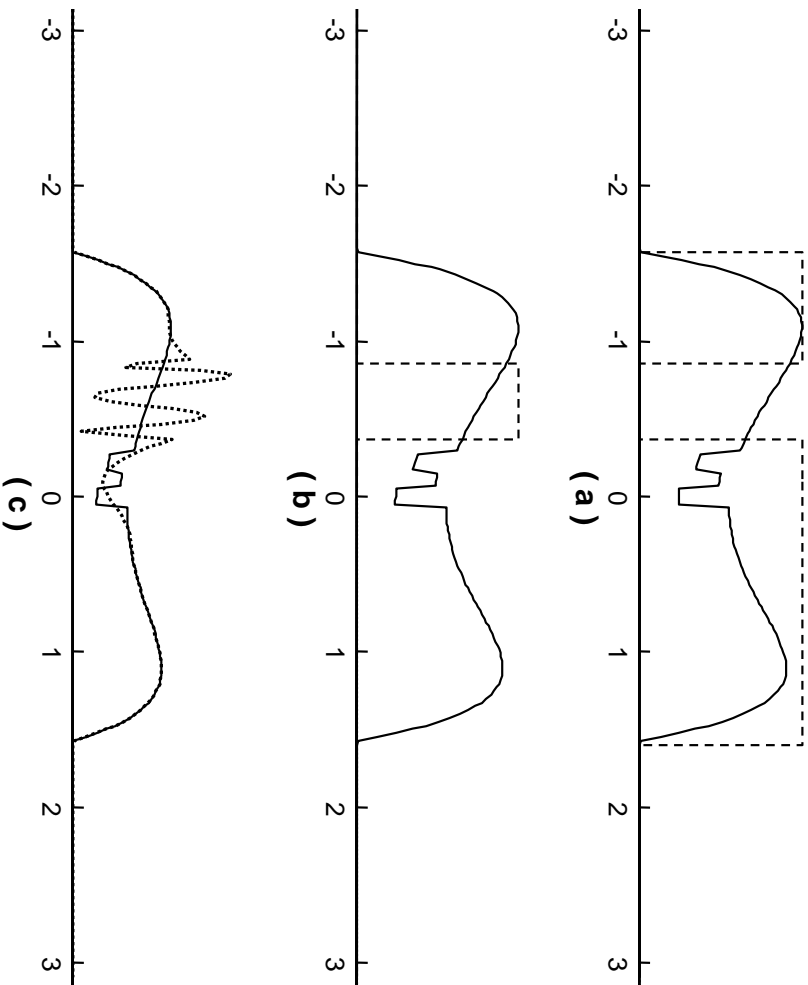


Fig. 6. An example of reconstructing a one-dimensional object function (solid line) using a properly-sized but improperly-located window as  $X_S$  ( $X_S$  does not cover the small portion of interest at all) in our proposed method, (a) the window function  $X_L$  (dashed line), (b) the window function  $X_S$  (dashed line), and (c) the best estimate (dotted line) with window functions  $X_L$  in (a) and  $X_S$  in (b). Shieh\_06.eps

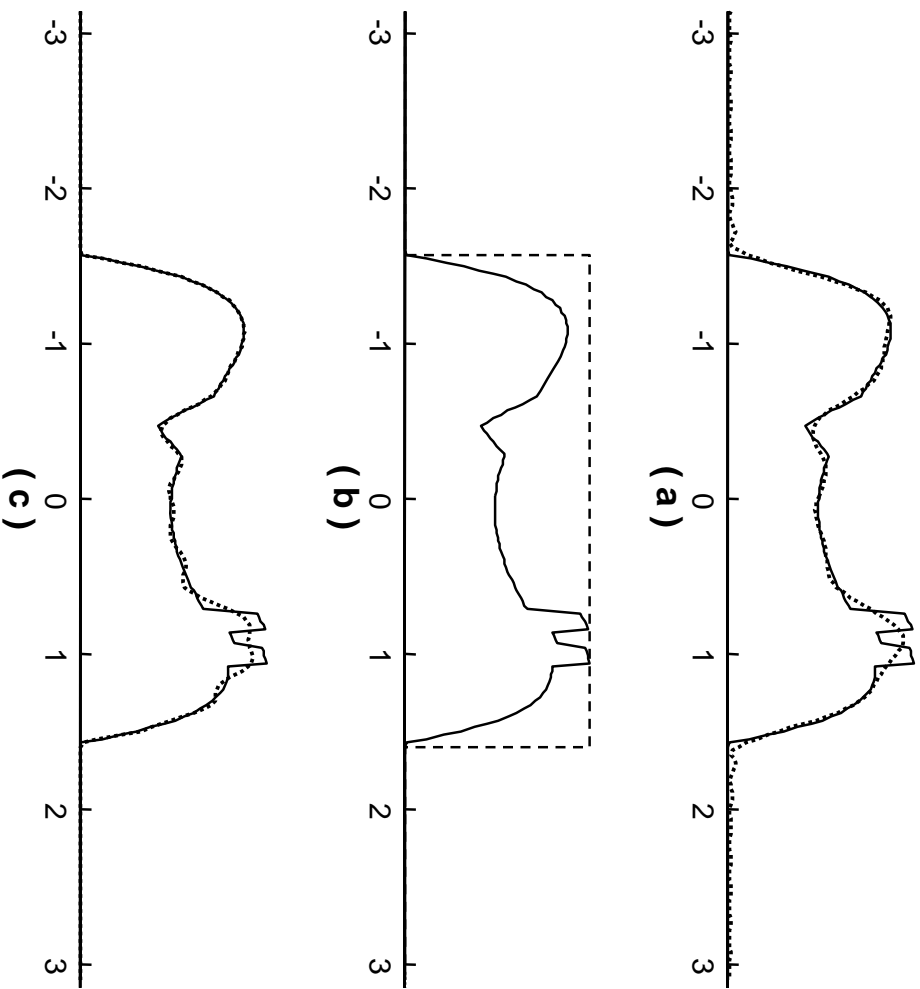


Fig. 7. An example of reconstructing a one-dimensional object function (solid line) by the DFT and PDFT, (a) the DFT estimate (dotted line), (b) the prior function (dashed line), and (c) the PDFT estimate (dotted line) with the prior in (b). Shieh\_07.eps

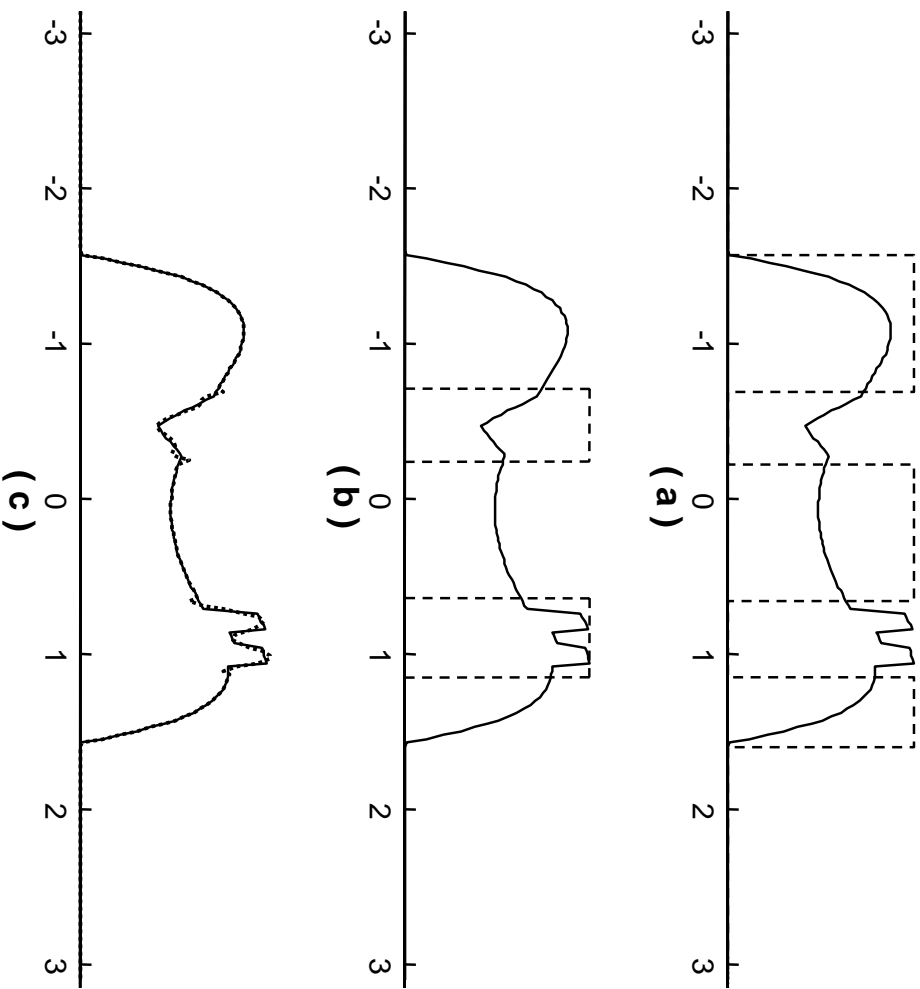


Fig. 8. An example of reconstructing a one-dimensional object function (solid line) by our proposed method, (a) the window function  $\chi_L$  (dashed line), (b) the window function  $\chi_S$  (dashed line), and (c) the estimate by our proposed method (dotted line) with  $\chi_L$  in (a) for complex exponentials of frequencies  $\{-7, \dots, 0, \dots, 7\}$  and  $\chi_S$  in (b) for otherwise. Shieh\_08.eps

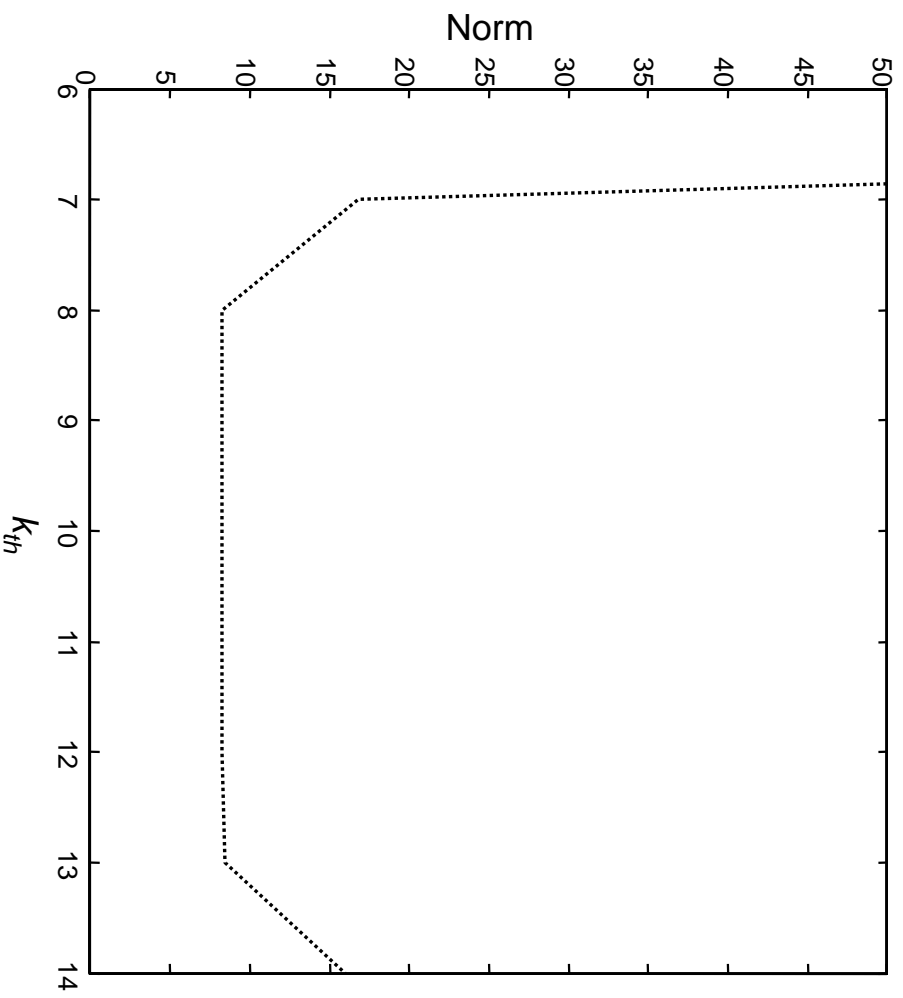


Fig. 9. The norms of the image estimate by our proposed method with respect to  $k_{th}$  for the example in Fig. 2. Shieh\_09.eps

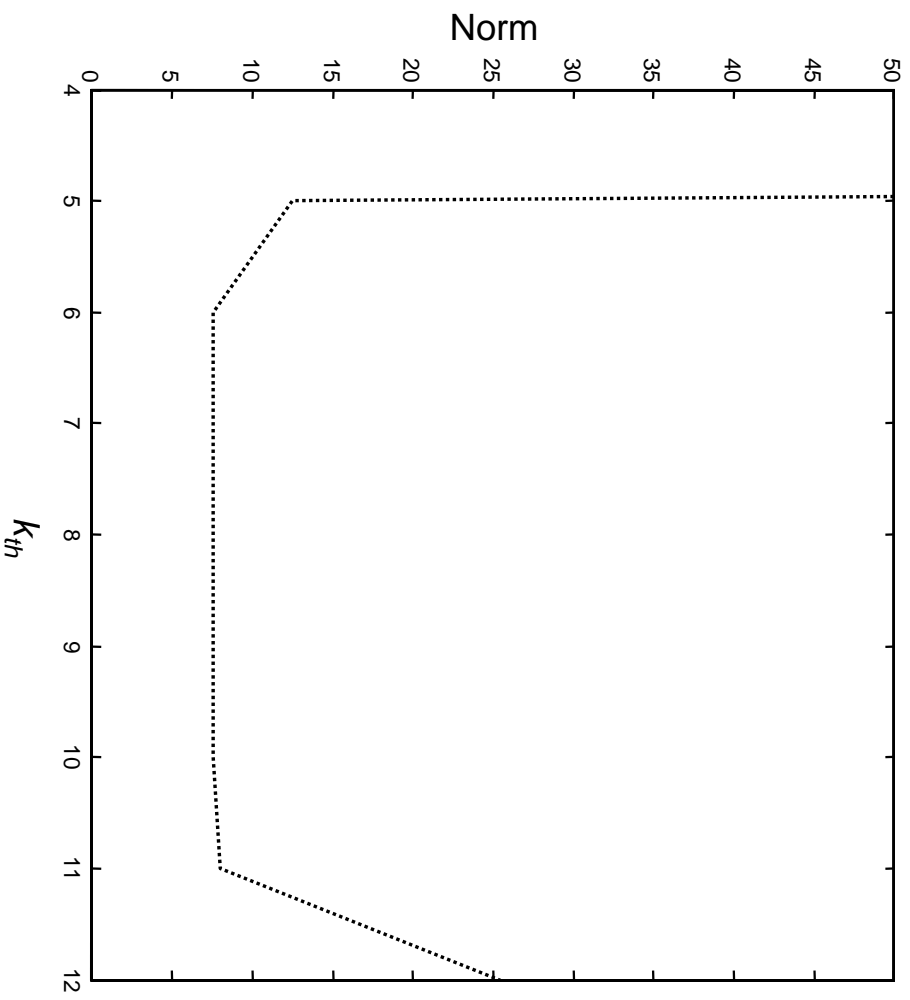


Fig. 10. The norms of the image estimate by our proposed method with respect to  $k_{th}$  for the example in Fig. 8. Shieh\_10.eps

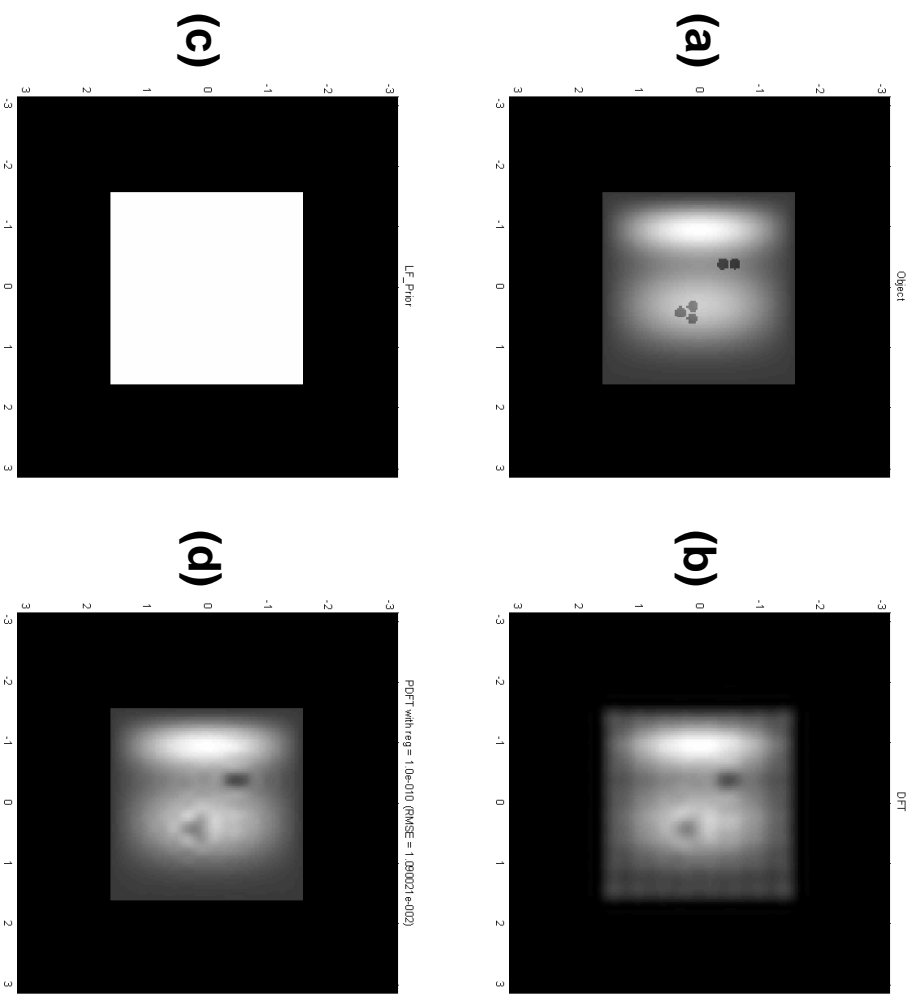


Fig. 11. An example of reconstructing a two-dimensional object function by the DFT and PDFT, (a) the object, (b) the DFT estimate, (c) the prior function, and (d) the PDFT estimate with the prior in (c). Shieh-11.eps

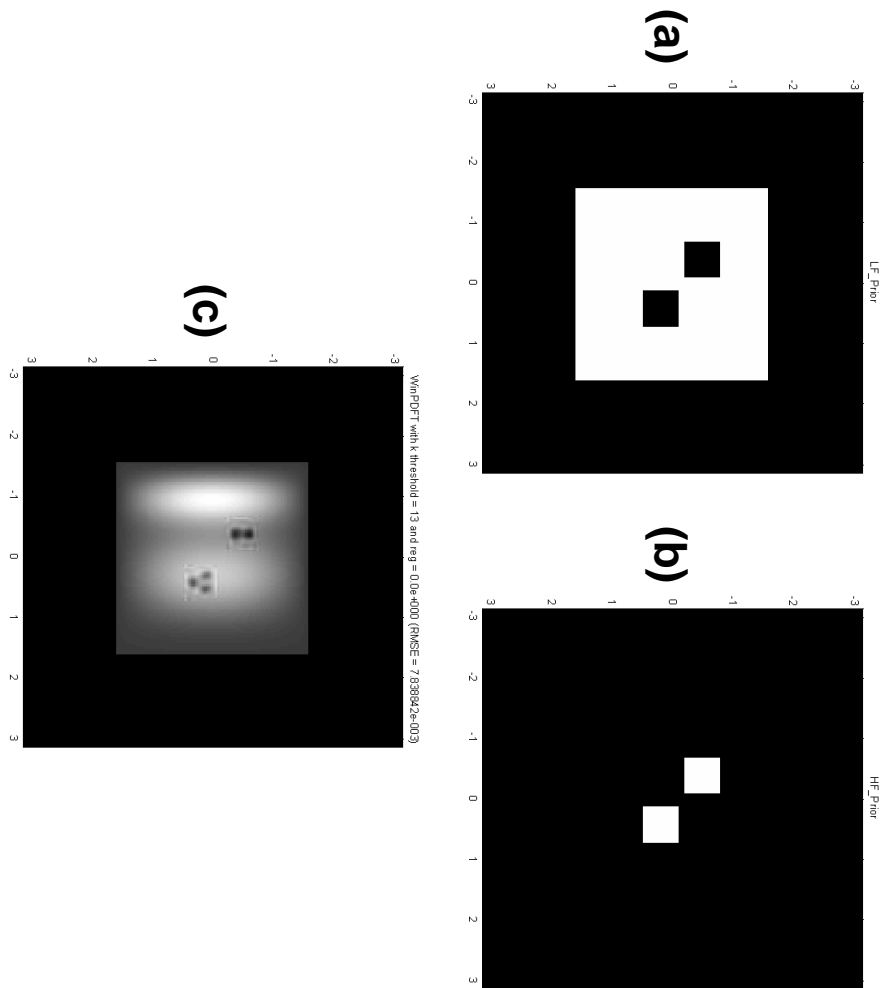


Fig. 12. An example of reconstructing a two-dimensional object function by our proposed method, (a) the window function  $\chi_L$ , (b) the window function  $\chi_S$ , and (c) the estimate by our proposed method with  $\chi_L$  in (a) for complex exponentials  $\{(\alpha_m, \beta_n) \mid \sqrt{\alpha_m^2 + \beta_n^2} \leq 13, \text{ for } m = 1, 2, \dots, M \text{ and } n = 1, 2, \dots, N\}$  and  $\chi_S$  in (b) for otherwise. Shieh\_12.eps